Diffusion-controlled radiochemical oxidation of bisphenol A polysulfone

Emmanuel Richaud,[a,b]* Xavier Colin,[a] Carole Monchy-Leroy,[b] Ludmila Audouin[a] and Jacques Verdu[a]

Abstract

The radiochemical degradation of bisphenol A polysulfone was investigated under a γ-ray dose rate of 24 kGy h^{-1} up to 30.7 MGy total absorbed dose at 60 °C using gel permeation chromatography, sol–gel analysis, glass transition and rheometry measurements, and oxidation profile measurements by microscopy coupled with Fourier transform infrared analysis in attenuated total reflectance mode. Thin (200 μm) and thick (2 mm) samples were compared. Thin samples undergo mainly chain scissions whereas thick ones undergo mainly crosslinking. The thickness of oxidized layers and, radiochemical yields for chain scissions, crosslinking, oxygen absorption and radical formation were tentatively determined from experimental data in order to determine the influence of oxidative processes on radiochemical ageing and to establish the nature of the crosslinking reactions.

Keywords: bisphenol A polysulfone; radiochemical ageing; crosslinking; chain scissions; glass transition

INTRODUCTION

Bisphenol A polysulfone (PSU) is widely used in nuclear plant engineering due to its interesting electrical insulation and mechanical performances at relatively high temperatures. Moreover, a relatively high resistance to ionizing radiations is expected owing to its aromatic character. PSU undergoes both chain scissions and crosslinking. The competition between these two phenomena depends on dose rate and temperature.[1–4] This paper is dedicated to this duality through a comparison between thin and thick samples exposed to radiation in air at moderate temperature. The crosslinking mechanism remains unclear since some authors suggest an H-crosslinking mode[3,4] whereas more recent studies have shown a Y-crosslinking mode.[5,6] The present work is hence aimed at bringing new insights into this mechanism by comparing results obtained from classic analytical tools (gel permeation chromatography (GPC), sol–gel analysis[7]), and less classic ones (molar mass changes from glass transition temperature (T_g) measurements,[8] rheometry,[9] attenuated total reflectance (ATR) microscopy[10,11]); and by establishing the nature of PSU reactive sites using Fourier transform infrared (FTIR) spectroscopy in transmission mode.[12]

EXPERIMENTAL

Samples

The material used in the study was a commercial Udel 1700 grade PSU supplied by Solvay Chemicals. GPC analysis gave number-average molar mass $M_N = 31.0\ kg\ mol^{-1}$ and weight-average molar mass $M_W = 48.8\ kg\ mol^{-1}$ (see below). Initial T_g value from DSC analysis was close to 189 °C. Thin samples were obtained by pressing pellets into 200 μm films at 240 °C during 60 s using a laboratory press (Gibrite). Thick samples were injection-moulded using the following processing conditions: $T_{nozzle} = 380$ °C, $T_{zone2} = 375$ °C, $T_{zone3} = 360$ °C, $T_{zone4} = 355$ °C, $T_{zone5} = 350$ °C, $T_{zone6} = 340$ °C, commutation pressure = 110 MPa, hold pressure = 110 MPa, hold time = 4 s, cooling time = 16 s, screw speed = 40 rpm, injection rate = 10 mm s^{-1}. Samples were machined into rectangular specimens of 7.5 cm × 2.25 cm × 0.2 cm (approximate). Pellets were dried (16 h at 135 °C) prior to processing, according to supplier recommendations.

Some comparisons with previously studied poly(ether ether ketone) (PEEK)[10] are also presented.

Characterization

DSC measurements

The thermal characteristics were investigated using a DSC Q10 apparatus (TA Instruments) after calibration with an indium standard. Samples of approximately 10 mg were analysed from 25 and 250 °C at a from 25 to 250 °C at a 10 °C min^{-1} scanning rate. Sufficiently thin PSU sheets were placed in aluminium pans covered with a lid in order to minimize temperature gradients within the sample. T_g was determined as the inflexion point of the thermograms.

Rheometric measurements

Rheometric measurements in the molten state were made in oscillatory mode using an ARES apparatus (Rheometrics Scientific)

* *Correspondence to: Emmanuel Richaud, Arts et Metiers ParisTech, CNRS, PIMM, 151 boulevard de l'Hôpital, 75013 Paris, France.*
E-mail: emmanuel.richaud@paris.ensam.fr

a *Arts et Metiers ParisTech, CNRS, PIMM, 151 boulevard de l'Hôpital, 75013 Paris, France*

b *EDF R&D, Département Matériaux et Mécanique des Composants, Avenue des Renardières, Ecuelles, 77818 Moret sur Loing, France*

in a plane–plane configuration with 25 mm diameter plates separated by a 1 mm gap. Real and imaginary components of complex viscosity η^* and complex shear modulus G^* were recorded at 220 °C in the 10^{-2}–10^2 rad s^{-1} angular frequency range.

GPC measurements

Samples were analysed using a GPC system comprising a Waters HPLC apparatus with a Styragel SE5 column with a tetrahydrofuran (THF) flow rate of 0.5 mL min^{-1} and UV detection at 254 nm. The column and detector temperatures were, respectively, 40 and 35 °C. Aliquots were prepared by dissolving samples of *ca* 15 mg in 10 mL of THF (analytic grade supplied by Carlos Erba). The injection volume was 10 µL. Data were acquired and analysed using Breeze software. The column was calibrated using monodisperse polystyrene (PS) samples of molar mass ranging from 3.07 to 3730 kg mol^{-1}. PS equivalent molar masses were then converted into PSU ones using the universal calibration method[13] according to which two polymers having different molar mass can have the same elution time provided their intrinsic viscosities are linked by the following relationship:

$$\ln M_{PSU} = \frac{1}{1+\alpha_{PSU}} . \ln \frac{k_{PS}}{k_{PSU}} + \frac{1+\alpha_{PS}}{1+\alpha_{PSU}} . \ln M_{PS} \qquad (1)$$

where k_{PS}, α_{PS}, k_{PSU} and α_{PSU} are PS and PSU Mark–Houwink parameters for a given solvent at a given temperature.

Unfortunately, Mark–Houwink coefficients for PSU in THF are not available in general monographs dedicated to liquid chromatography[14] or even in research papers in which PS–PSU conversion is used.[7,15] This led us to use the coefficients of a polymer having the same characteristics as PSU. The best candidate should have the same viscosity as a PSU of the same molar mass. Since

$$[\eta] = \frac{V_h}{M} \qquad (2)$$

where $V_h = \phi \times \langle r^2 \rangle_0^{3/2}$ is the hydrodynamic volume of a chain in solution, we concluded that both polymers should have the same end-to-end distance for a given molar mass, i.e. the same chain characteristic ratio c_∞. Bisphenol A polycarbonate (PC) appeared then as a good choice. Its Mark–Houwink coefficients in THF at 25 °C are $k = 3.99 \times 10^{-4}$ dg L^{-1}, $\alpha = 0.77$, so that

$$M_{PSU} = 0.597 \times M_{PS}^{0.96} \qquad (3)$$

Applying this relationship, $M_N = 31.0$ kg mol^{-1}, $M_W = 48.8$ kg mol^{-1} and dispersity $Đ = M_W/M_N = 1.57$ were calculated for as-received PSU. These values are consistent with previously reported ones for a PSU of similar grade[7,16] and in any case are in better agreement than those obtained directly using PS calibration ($M_N = 82.5$ kg mol^{-1}, $M_W = 134.5$ kg mol^{-1}, $Đ = 1.63$).

Sol–gel analysis

Sol–gel analysis was carried out by solvent swelling with chloroform at room temperature. Samples of 0.15 g (m_0) were immersed in approximately 20 mL chloroform during 24 h. After this duration, the insoluble fraction was filtered, dried in a vacuum oven at 60 °C overnight and then weighed (m_I). The gel content was calculated as the ratio m_I/m_0.

FTIR analysis

Analysis in transmission mode. Free-standing films were analysed in transmission mode using an IFS 28 apparatus (Brucker). Spectra were obtained by the averaging of 32 scans at 4 cm^{-1} resolution.

Analysis in ATR mode. Thick samples processed by injection moulding were analysed in ATR mode using an IFS 28 apparatus (Brucker) equipped with a diamond crystal. Spectra were obtained by the averaging of 32 scans at 4 cm^{-1} resolution.

ATR microscopy. The thickness of oxidized layers was estimated using micro-ATR infrared spectroscopy with a Spotlight 300 microscope apparatus coupled with a Spectrum 100 FTIR spectrophotometer (PerkinElmer) driven by Spectrum Image software. Samples were analysed with a germanium crystal. The spectra were obtained at 4 cm^{-1} minimum resolution, with a pixel size equal to 1.56 µm. Two scans per pixel were recorded. Thick samples were embedded in a commercial epoxide-amine resin. After curing, the samples were polished with 400 and 4000 granulometry discs under a cold water flow before PSU cross-section analysis. An example of an interface image is shown in Fig. 1(a). The rectangle delimits the investigated zone (here 1000 µm × 200 µm) in which edge regions cannot be reliably analysed. The characteristic PSU absorption at 1145 cm^{-1} due to antisymmetric stretching ν_{AS} of SO_2 groups (Fig. 1(b)) was used to locate precisely the epoxy–PSU interface. Typical infrared mapping (Fig. 1(c)) was obtained by an analysis in 'single cm^{-1} mode' at 1145 cm^{-1}. The changes due to oxidation were then estimated from the absorbance ratio at 1730 cm^{-1} (oxidation products, see later) and 1145 cm^{-1}.

Optical microscopy

Optical microscopy images were acquired using a BH2 microscope (Olympus) driven by Archimed software.

Exposure conditions

Irradiations were carried out using a ^{60}Co γ-ray source at 60 °C under 0.15 MPa air pressure (Brigitte device, SCK-CEN, Mol, Belgium) at 24 kGy h^{-1} dose rate. Statistical chain scissions concentration in Red Perspex (poly(methyl methacrylate)) allowed the total emitted dose to be measured with an error of less than 5%.

RESULTS

Sol–gel analysis

We were interested in comparing PSU with a previously studied PEEK sample[10] exposed under the same conditions:

- Thin PSU films (200 µm) remain totally soluble and their gel content remains equal to zero even at high radiation doses.
- PEEK samples having about the same thickness (250 µm) undergo gelation while thinner samples (60 µm) remain soluble.
- Thick PSU samples (2 mm) become partially insoluble at doses higher than 2.0 MGy.

Figure 2 shows the results for insoluble fraction *versus* dose for thick PSU samples (2 mm) and thick PEEK samples (250 µm). The differences appear clearly:

- The gelation dose is lower for PSU (*ca* 1–2 MGy) than for PEEK (5–10 MGy).
- Gelation occurs suddenly for PSU and progressively for PEEK.

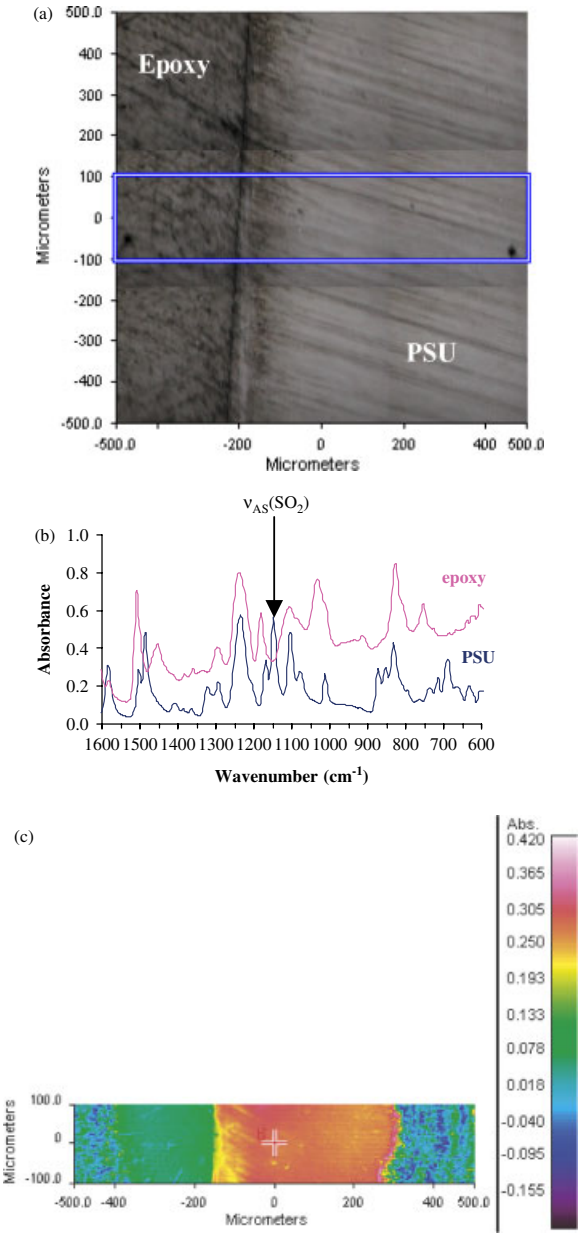

Figure 1. Profiles obtained using ATR microscopy. (a) Image of analysed sample at the PSU–epoxy interface. (b) FTIR spectra of epoxy and PSU. (c) Localization of PSU sample using 1145 cm^{-1} absorption. One sees the 'edge effect' preventing analysis of the regions of the x-axis of $x < -400$ μm or $x > 400$ μm.

- PSU becomes nearly insoluble at the highest dose whereas PEEK soluble fraction remains about 20% at 30.7 MGy. In fact, as will be seen later, about 10% of polymer is oxidized at the maximal absorbed dose and remains soluble. The asymptotic value reached for PSU is probably closer to 90% than 100%.

The radiochemical yields for chain scissions $G(s)$ and crosslinking $G(x)$ in thick samples were tentatively determined using the Charlesby–Pinner equation.[17] First, we supposed an H-crosslinking mode. The corresponding equation is

$$w_S + w_S^{1/2} = \frac{G_H(s)}{2G_H(x)} + \frac{10^7}{M_{W0}.G_H(x).\delta} \quad (4)$$

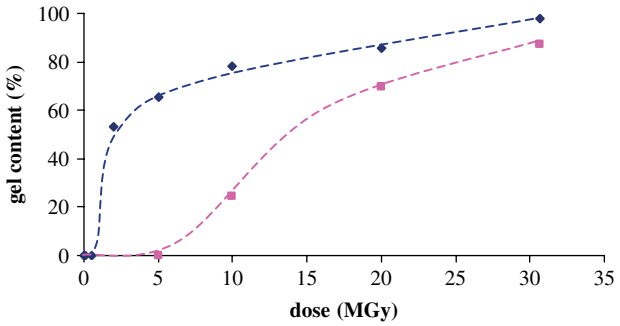

Figure 2. Gel content changes of thick PSU (♦) and PEEK (■) samples for various irradiation doses.

where $w_S = 1 - w_I$ is the soluble fraction; $G_H(s)$ and $G_H(x)$ are the radiochemical yields expressed for 100 eV for chain scissions and crosslinking, respectively, for an H-crosslinking mechanism; δ is the dose (Gy); and M_{W0} is the initial weight-average molar mass (kg mol^{-1}). A plot of $w_S + w_S^{1/2}$ against δ^{-1} is reasonably close to a straight line (Fig. 3(a)) whose slope and intersect at the origin give, respectively, $G_H(x) = 0.157$ and $G_H(s) = 0.173$.

Second, we assumed a Y-crosslinking mode, for which the Charlesby–Pinner equation is

$$1 + 3w_S^{1/2} = \frac{2G_Y(s)}{2G_Y(x)} + \frac{1.93 \times 10^7}{M_{N0}.G_Y(x).\delta} \quad (5)$$

A plot of $1+3w_S^{1/2}$ *versus* δ^{-1} is also approximately linear (Fig. 3(b)). This gives $G_Y(x) = 0.335$ and $G_Y(s) = 0.368$.

GPC measurements of molar mass changes

Since thick samples soon become insoluble, only thin films were analysed using GPC. Figure 4(a) shows some chromatograms. The molar mass decreases regularly with dose. The dispersity remains almost constant, which indicates the absence of marked heterogeneity of the chain scissions process and of crosslinking. As a matter of fact, the 'radiochemical translation' of Saito's equations can be used.[18] First, for an H-crosslinking mode:

$$\frac{1}{M_N} - \frac{1}{M_{N0}} = 10^{-7} \times [G_H(s) - G_H(x)] \times \delta \quad (6)$$

$$\frac{1}{M_W} - \frac{1}{M_{W0}} = 10^{-7} \times \left[\frac{G_H(s)}{2} - 2G_H(x)\right] \times \delta \quad (7)$$

Reciprocal molar masses $1/M_N$ and $1/M_W$ can be plotted against dose (Fig. 4(b)). The slope values give $G_H(s) \approx 0.17$ (in good agreement with sol–gel analysis of thick samples) and $G_H(x) \approx 0$ for thin films. The dispersity $Đ$ is initially close to 1.48 and tends towards 2 as expected for a homogenous random chain scissions process.

Second, for a Y-crosslinking mode:

$$\frac{1}{M_N} - \frac{1}{M_{N0}} = 10^{-7} \times [G_Y(s) - G_Y(x)] \times \delta \quad (8)$$

$$\frac{1}{M_W} - \frac{1}{M_{W0}} = 10^{-7} \times \left[\frac{G_Y(s)}{2} - G_Y(x)\right] \times \delta \quad (9)$$

Here, the experimental results give $G_Y(s) = 0.17$ and $G_Y(x) \approx 0$.

It is noteworthy that both sets of values (differing by the crosslinking scenario) are very close in thin films whereas they are

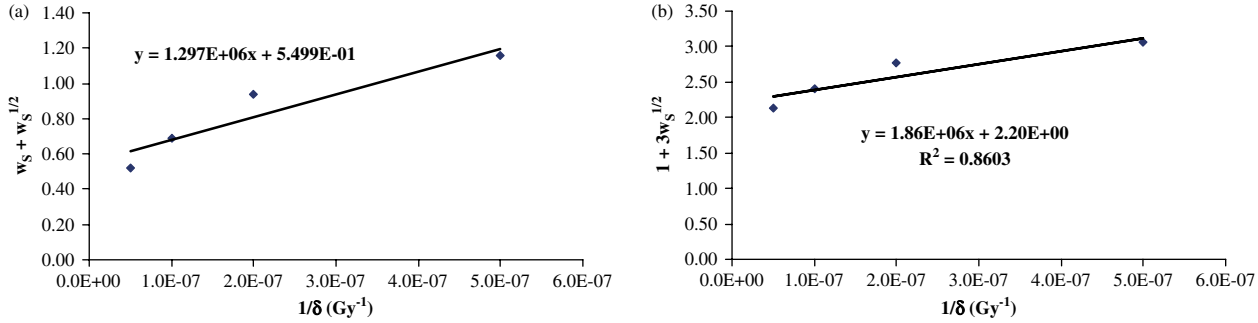

Figure 3. Charlesby–Pinner plots for (a) H-crosslink mode and (b) Y-crosslink mode.

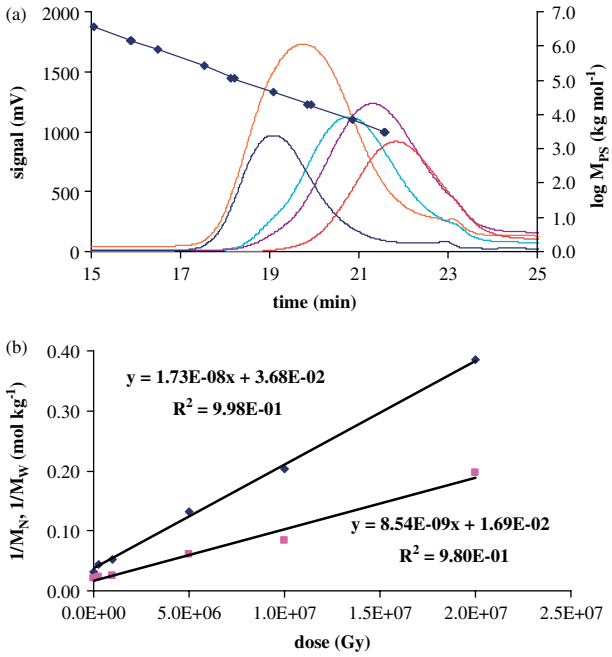

Figure 4. (a) Chromatograms of thin PSU samples (left-hand axis) for various irradiation doses and calibration with PS standards (♦; right-hand axis). (b) Assessment of $G(x)$ and $G(s)$.

significantly different for thick ones. This suggests that the nature of the crosslinking mechanism would have a lower influence on molar mass changes in the case of thin samples than in the case of thick samples.

It should be mentioned here that various versions of the Saito[5,6,19,20] and Charlesby–Pinner[5,6,21,22] equations for H- or Y-crosslinking can be found in the literature. We have chosen the versions fulfilling the condition to give the same expression of gelation doses. Assuming a homogeneous process in a first approach, the gelation dose (δ_G) would be given by the following expressions.

$$\text{For H-crosslinking}: \quad \delta_G = \frac{2 \times 10^7}{M_{W0}[4G_H(x) - G_H(s)]} \tag{10}$$

whether using $w_S = 1$ in Eqn (4) or $1/M_W = 0$ in Eqn (7).

$$\text{For Y-crosslinking}: \quad \delta_G = \frac{2 \times 10^7}{M_{W0}[2G_Y(x) - G_Y(s)]} \tag{11}$$

whether using $w_S = 1$ in Eqn (5) or $1/M_W = 0$ in Eqn (9).

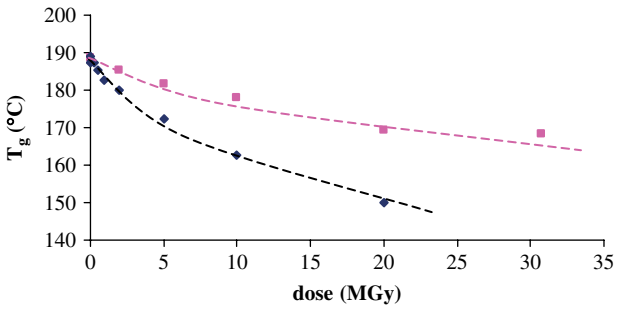

Figure 5. T_g changes with dose for thin films (♦) and thick samples (■).

DSC measurements of glass transition temperature

T_g decreases almost linearly with time for both 2 mm and 200 µm thick samples, but the decrease is faster for thin samples (Fig. 5) than for thick samples. This is not surprising since T_g decreases with chain scissions and increases with crosslinking. Thus, it seems that crosslinking partially compensates the chain scissions effect in thick samples.

Case of thin films

Thin films undergo certainly a 'pure' random chain scissions process (consistent with GPC results) for which $G(s)$ yield can be derived from the Fox–Flory relationship:[23]

$$T_g = T_{g\infty} - \frac{k_{FF}}{M_N} \tag{12}$$

where the Fox–Flory constant k_{FF} is a parameter characterizing the chemical structure.

According to our interpretation of GPC results, it seems that the crosslinking concentration x is very low compared to the chain scissions one, so that Eqn (6) becomes

$$\frac{1}{M_N} - \frac{1}{M_{N0}} = s \tag{13}$$

Since

$$\frac{ds}{dt} = 10^{-7} \times G(s) \times I \tag{14}$$

one can write

$$\frac{dT_g}{d\delta} = -k_{FF} \times 10^{-7} \times G(s) \tag{15}$$

The PSU Fox–Flory constant value is required for calculating $G(s)$ from T_g decrease. Parameter k_{FF} can be estimated in many ways.

The first one is derived from the 'free volume' theory. If $T_{g\infty}$ is the T_g value for a hypothetical polymer of infinite molar mass, the volume excess of a finite-molar-mass polymer at $T_{g\infty}$ is proportional to the number of chain ends. This gives

$$k_{FF} = \frac{2\rho V_{end}}{\Delta\alpha} \tag{16}$$

where ρ is the density of amorphous polymer, V_{end} is the volume excess of one chain end and $\Delta\alpha = \alpha_L - \alpha_g$ is the difference between volume expansion coefficients in rubber/liquid state (α_L) and glassy state (α_g). The estimation is based on two hypotheses according to which, in a restricted family of polymers having close molecular structures,

- the Simha and Boyer rule[24] is valid: $\Delta\alpha_i T_{gi} =$ constant (for the ith polymer); and
- V_{end} is almost independent of the polymer structure.

Here, PSU is compared to PC, both polymers having similar characteristics (especially chain stiffness) and probably the same type of chain ends (hydroxyl groups). One can write

$$\frac{(k_{FF})_{PSU}}{(k_{FF})_{PC}} = \frac{\rho_{PSU}}{\rho_{PC}} \frac{(T_{g\infty})_{PSU}}{(T_{g\infty})_{PC}} \tag{17}$$

The second way of estimating k_{FF} is derived from a classical copolymer law which considers chain ends as comonomers:

$$\frac{M_N}{T_g} = \frac{M_N}{T_{g\infty}} + 2b \tag{18}$$

or

$$T_g = \frac{T_{g\infty}}{1 + 2b.T_{g\infty}/M_N} \tag{19}$$

where b is the contribution of a chain end to $M_N T_g^{-1}$. Using classical approximations one obtains

$$T_g = T_{g\infty} - \frac{2b.{T_{g\infty}}^2}{M_N} \tag{20}$$

so that

$$k_{FF} = 2bT_{g\infty}^2 \tag{21}$$

Under the assumption of structure-independent b parameter (here also in a reasonably restricted polymer family), one can write

$$\frac{(k_{FF})_{PSU}}{(k_{FF})_{PC}} = \left(\frac{(T_{g\infty})_{PSU}}{(T_{g\infty})_{PC}}\right)^2 \tag{22}$$

The third way of estimating k_{FF} is an empirical relationship proposed by Bicerano.[25] The following correlation was reported:

$$\frac{(k_{FF})_{PSU}}{(k_{FF})_{PC}} = \left(\frac{(T_{g\infty})_{PSU}}{(T_{g\infty})_{PC}}\right)^3 \tag{23}$$

Parameter $(T_{g\infty})_{PSU}$ is unknown. Since T_g values for PSU scatter between 178 and 189 °C,[26–30] it seems reasonable to assume that it is probably close to 463 K. Using $(k_{FF})_{PC} = 187$ K kg mol^{-1},[21] ρ_{PC} close to 1200 kg m^{-3}, ρ_{PSU} close to 1220 kg m^{-3} and $(T_{g\infty})_{PC} = 434$ K,[21] the three ways of estimating k_{FF} give, respectively, $(k_{FF})_{PSU} = 203$, 213 and 227 K mol kg^{-1}. The difference is insignificant in the frame of this work. We will choose arbitrarily the median value: $(k_{FF})_{PSU} \approx 227$ K kg mol^{-1}.

A graphical estimation (Fig. 5) gives for the thin samples

$$\frac{dT_g}{d\delta} \approx \frac{T_g(0\ \text{MGy}) - T_g(5.0\ \text{MGy})}{5.0 \times 10^6} = -3.2 \times 10^{-6}\ \text{K Gy}^{-1} \tag{24}$$

from which one obtains $G(s) \approx 0.15$, which is close to the previous estimation from GPC measurements for thin films (Y- or H-crosslinking mode) and sol–gel analysis in the case of H-crosslinking mode.

Sol–gel analysis applied to the Y-crosslinking mode gives $G(s) \approx 0.37$. According to Eqn (15), this value would be consistent with experimental data provided that $k_{FF} \approx 80$ K kg mol^{-1}. Since k_{FF} is clearly an increasing function of $T_{g\infty}$, and since k_{FF} is close to 100 K kg mol^{-1} for PS ($(T_{g\infty})_{PS}$ is equal to 373 K), no doubt $(k_{FF})_{PSU} \approx 80$ K kg mol^{-1} is unrealistic. In conclusion, T_g measurements are consistent with $G(s) \approx 0.1$–0.2 rather than $G(s) \approx 0.3$–0.4. In other words, the hypothesis of Y-crosslinking mode must be rejected.

Case of thick samples

Sol–gel analysis proves that PSU undergoes crosslinking and that chain scissions occur at almost the same rate (Charlesby–Pinner approach gives $G_H(s)/G_H(x) \approx G_Y(s)/G_Y(x) \approx 1$). The observed T_g decrease for thick samples suggests that the influence of crosslinking is partially compensated (and even dominated) by the simultaneous chain scissions. Let us try to model the influence of combined chain scission and crosslinking on T_g changes.

For ideal networks having no dangling chains, the effect of crosslinking on T_g obeys the DiMarzio's law:[31]

$$T_g = \frac{T_{gl}}{1 - k_{DM} F \nu} \tag{25}$$

where T_{gl} is the glass transition temperature for uncrosslinked polymer. Here, it seems reasonable to consider $T_{gl} \approx 463$ K (i.e. the value for a hypothetical PSU sample of infinite molar mass). F is a flex parameter equal to the average molar mass per rotatable unit. Here, $F_{PSU} = 0.1105$ kg mol^{-1}. k_{DM} parameter is the DiMarzio's constant and is close to unity. Finally, ν is the elastically active chain concentration. For ideal networks resulting from H-crosslinking

$$\nu = 2x \tag{26}$$

where x is the crosslinking concentration. Supposing that the DiMarzio's equation can be applied for non-ideal networks, Eqn (25) becomes the Fox–Loshaek equation for low crosslinking density:[32]

$$T_g = T_{gl} + k_{FL} x \tag{27}$$

with the Fox–Loshaek constant k_{FL} being given by

$$k_{FL} = 2T_{gl} F k_{DM} \tag{28}$$

so that $k_{FL} \sim 102$ K kg mol^{-1}.

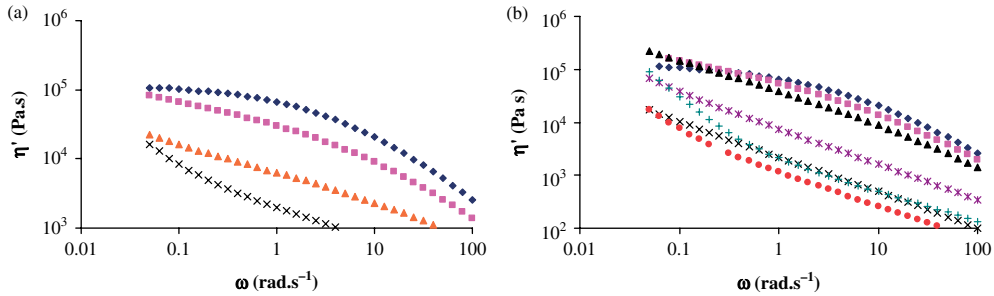

Figure 6. Changes in real viscosity component with angular frequency ω: (a) films before (♦), and after 0.096 MGy (■), 0.5 MGy (▲) and 5.0 MGy (×); (b) thick samples before (♦), and after 0.096 MGy (■), 0.5 MGy (▲), 2.0 MGy (×), 5.0 MGy (✳), 10.0 MGy (●) and 20.0 MGy (+).

Finally, the global changes of T_g would be given by

$$\frac{dT_g}{d\delta} = \left(\frac{\partial T_g}{\partial s}\right)\frac{ds}{d\delta} + \left(\frac{\partial T_g}{\partial x}\right)\frac{dx}{d\delta} \quad (29)$$

so that

$$\frac{dT_g}{d\delta} = 10^{-7}[k_{FL}G(x) - k_{FF}G(s)] \quad (30)$$

Using $G(s) \approx 0.15$ and $G(x) \approx 0.15$, one obtains

$$\frac{dT_g}{d\delta} = -1.7 \times 10^{-6}\ \text{K Gy}^{-1}$$

This value is consistent with the experimental observations, showing that the rate of decrease of T_g with dose for thick samples is twice that for thin ones. It is worth highlighting that only $G(s)$ and $G(x)$ values obtained for H-crosslinking with physically reasonable k_{FF} and k_{FL} values allow this trend to be simulated.

Rheological measurements

In the case of thin samples, irradiation results in a global decrease of the real component of viscosity η' (Fig. 6(a)), as expected for a chain scission process. As for T_g, the fact that the rate of change of η' decreases with time would be explained by the occurrence of some branching resulting from crosslinking events. Even if crosslinking is undoubtedly minor in thin films, it seems that the presence of minor branching strongly modifies the shape of viscosity–frequency plots and could lead to the disappearance of the Newtonian plateau. By deriving the scaling law $\eta_0 = kM_W^{3.4}$, η_0 being the limit of η' when $\omega \to 0$, $G(s)$ can be roughly estimated. This value is of the same order of magnitude as that previously observed ($G(s) \approx 0.1$).

In the case of thick samples, the most striking fact is the disappearance of the Newtonian plateau at low doses (Fig. 6(b)). In the viscoelastic region ($\omega > 1$ rad s^{-1}), the viscosity first increases slightly at low doses and then decreases to be divided by a factor higher than 100 at a dose of 20.0 MGy.

The use of the Winter and Chambon approach[33] has been attempted to determine gelation dose from these results. It is considered here that whatever the degree of conversion of the crosslinking process, the real (G') and imaginary (G'') parts of the complex shear modulus G^* are linked to the angular frequency by a power law:

$$G'(\omega) = a\omega^{n'} \quad (31)$$

$$G''(\omega) = b\omega^{n''} \quad (32)$$

where n' and n'' are determined from rheometric data and are plotted *versus* dose in Fig. 7. Both curves intersect at the gel point. This corresponds here to a dose $\delta_G \approx 2.0$–3.0 MGy for thick samples, which is slightly higher than the value obtained from sol–gel analysis (Fig. 2). We then tried to compare this value with the one estimated from Eqns (10) and (11) using yield values $G(x) \approx G(s) \approx 0.15$ for H-crosslinking mode and 0.35 for Y-crosslinking mode. In every case, gelation dose is found close to 1 MGy, i.e. lower than the experimental value. One concludes that rheometry allows one to detect gelation, but not to establish the crosslinking mechanism. It is also interesting to note that T_g changes are more influenced by chain scissions than crosslinking, whereas the presence of crosslinking, or even short branching, strongly modifies the shape of the rheograms.

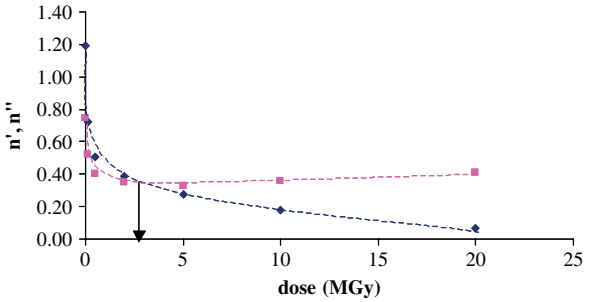

Figure 7. Changes of exponents n' (♦) and n'' (■) with dose and determination of sol–gel transition (arrow).

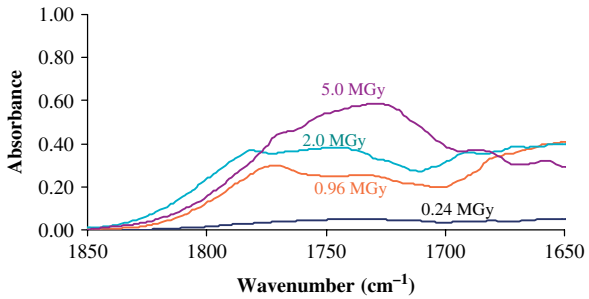

Figure 8. FTIR spectra in transmission mode of 200 µm thick PSU free-standing films after various irradiation doses.

Thickness of oxidized layer measurements

Infrared spectral analyses were performed on free-standing films in transmission mode or on thick sample surfaces in reflection mode. A broad increase in the 1700–1800 cm^{-1} region of the spectra is observed (Fig. 8). Many signals actually display a very

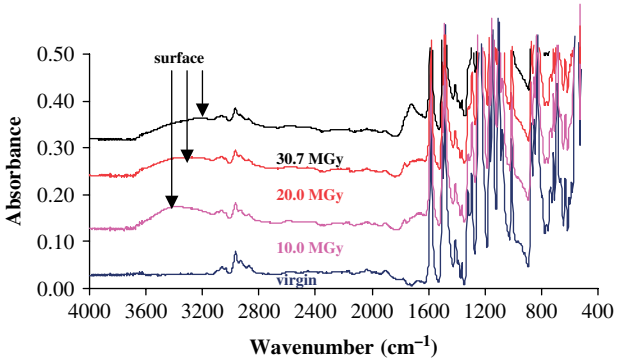

Figure 9. ATR spectra of exposed surface (solid curves) and bulk (dashed curves) of 2 mm thick virgin or irradiated PSU samples.

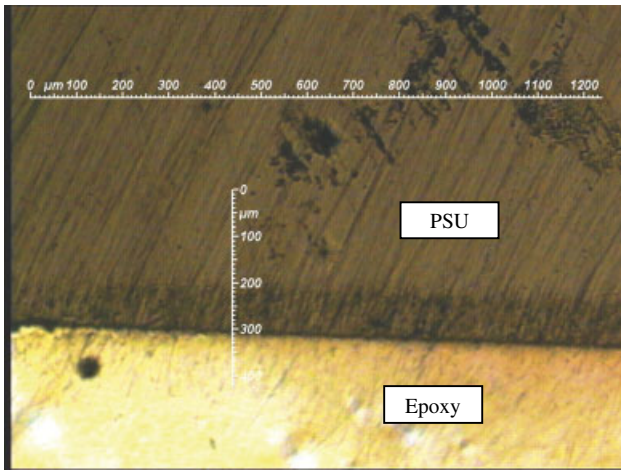

Figure 10. Optical microscopy image of PSU irradiated at 30.7 MGy.

large absorbance corresponding to saturation, which prevents us from a reliable quantitative analysis. That is the reason why we just present the spectral changes for low absorbed doses, and we do not attempt any quantitative reasoning aimed at establishing the mechanism based on carbonyl yields for instance.

The maximal absorbance is close to 1725 cm^{-1} with a shoulder at 1690 cm^{-1}. These signals are typically attributed respectively to aliphatic and aromatic ketones or aldehydes. It seems unquestionable that carbonyls come from an oxidative mechanism initiated by the abstraction of hydrogen belonging to isopropylidene groups.

For thick samples, the comparison of surface and bulk region analyses is indicative of an oxidized surface (presence of hydroxyl in the 3000–3800 cm^{-1} region, possibly of sulfonic or sulfuric acid in the 2400–3200 cm^{-1} one and carbonyls in the 1600–1800 cm^{-1} one) and a non-oxidized bulk (Fig. 9).

These results show that oxidation is limited by oxygen diffusion. We then investigated the thickness of oxidized layer (TOL) by:

- Optical microscopy (Fig. 10): the analysis of the bulk of a sample irradiated at 30.7 MGy reveals a slight contrast between the superficial layer and the core zone of the sample. It seems reasonable to suppose that this contrast is caused by oxidation. Basing on this assumption, the TOL could be of the order of 100 μm.
- Micro-ATR spectroscopy: the changes of the absorbance at 1730 cm^{-1} (normalized by that at 1145 cm^{-1}) with depth are plotted in Fig. 11. The result confirms that the TOL is close to 100 μm.

From a simplified theory of diffusion-limited oxidation,[34] a rough estimation of oxygen consumption rate r_{OX} (mol L^{-1} s^{-1}) in films or surface layers of thick samples can be done:

$$r_{OX} = \frac{D_{O2}[O_2]_S}{TOL^2} \tag{33}$$

where D_{O2} is the oxygen diffusion coefficient in PSU at 60 °C (m^2 s^{-1}), TOL is expressed here in m and $[O_2]_S$ is the equilibrium concentration (mol L^{-1}) given by Henry's law:

$$[O_2] = s_{O2} \times P_{O2} \tag{34}$$

in which s_{O2} is the solubility coefficient of oxygen in PSU (mol L^{-1} Pa^{-1}) and P_{O2} is the partial oxygen pressure (here, samples were exposed at 0.15 MPa of air i.e. 0.03 MPa of oxygen).

Starting from the observation that transport properties of moderately polar polymers do not vary strongly from one polymer to another,[35] it is assumed in a first approach that PSU properties are similar to those to PC ones: $D_{O2} = 8.3 \times 10^{-12}$ m^2 s^{-1} at 60 °C, $s_{O2} = 3.8 \times 10^{-8}$ mol L^{-1} Pa^{-1} and $P_{O2} = 0.03 \times 10^6$ Pa. Hence, for a dose rate of 24 kGy h^{-1}: $r_{OX} \approx 9.5 \times 10^{-7}$ mol L^{-1} s^{-1}. The radiochemical yield for oxygen consumption would thus be of the order of[36]

$$G_{OX} = \frac{10^7 r_{OX}}{I} \tag{35}$$

where I is the dose rate (Gy s^{-1}). G_{OX} is hence let us recall that samples were irradiated under 1.5 bar (150 kPa) air pressure. G_{OX} is hence of the order of 1.4 (molecules per 100 eV). This value is expected to be higher than or equal to the yield of stable oxidation products. Oxidation products are almost totally extractable by chloroform (Fig. 12). This indicates a large predominance of chain scissions over crosslinking in the regions accessible to oxygen.

Let us emphasize that the Charlesby–Pinner analyses presented above were performed without deconvolution of oxidized edges and non-oxidized bulk. It seems that the TOL remains constant and close to 100 μm whatever the absorbed dose. This would lead to multiplication of gel content by a factor of about 1.1 which does not modify significantly calculated $G(s)$ and $G(x)$ yields values.

DISCUSSION

On the difference between thin and thick samples

In thin samples (200 μm)

Crosslinking is almost totally inhibited and D tends towards 2. Both results indicate that oxidation is almost homogeneous in the whole sample thickness. Hence the TOL is such as $2 \times TOL \geq 200$ μm which is confirmed from FTIR microscopy measurements: TOL is *ca* 100–150 μm (depending on the chosen criterion for defining TOL) in bulk samples.

In thick samples (2 mm)

Crosslinking and chain scissions have similar radiochemical yields ($G(s) \approx G(x) \approx 0.15$). Since $4G(x) > G(s)$, crosslinking predominates over chain scissions and the samples undergo gelation.

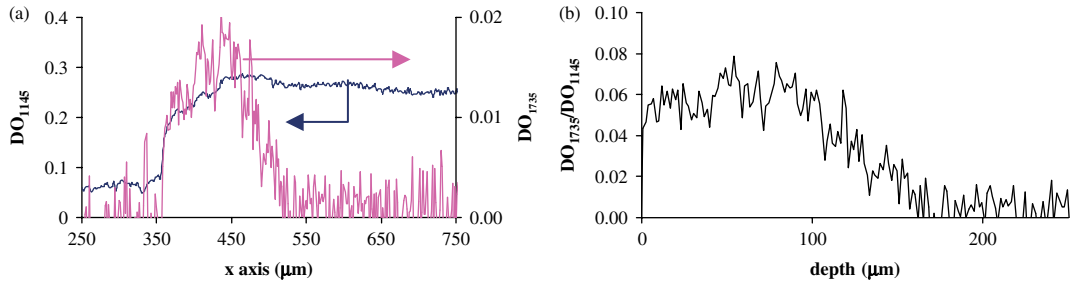

Figure 11. (a) Changes of absorptions at 1145 and 1735 cm^{-1} with position (arbitrary value, see Fig. 1). (b) Oxidation profiles; $x = 0$ corresponds to PSU wall.

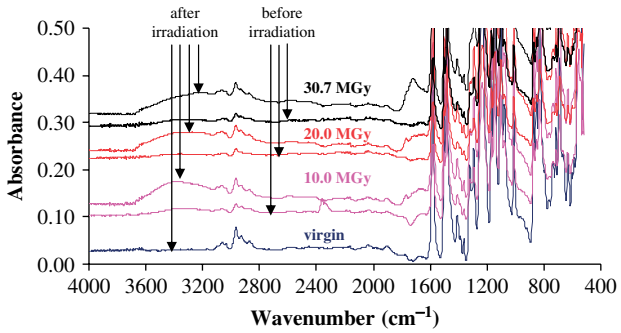

Figure 12. ATR spectra of exposed surface of 2 mm thick PSU samples before (solid curves lines) and after (dashed curves) extraction of soluble fraction by chloroform for various received doses.

On the crosslinking mechanism

The analysis of $G(s)$ and $g(x)$ measurements seems to indicate that H-crosslinking mode predominates at least for the studied experimental conditions (moderate temperature). Although NMR data would have been useful to establish this conclusion, the formation of aldehyde is in our mind a key argument: since hydrogen atoms are abstracted from isopropylidene groups, it is difficult to envisage that the so generated alkyl groups would react solely to give hydroperoxides and carbonyls without reacting together by coupling to crosslink. It is actually well documented that reaction between two alkyl radicals is the fastest of all reactions involved in radical chain mechanisms.[37] The corresponding radiochemical yields are $G(x) \approx G(s) \approx 0.15$.

On the difference of radiochemical reactivity between PEEK and PSU

Some previously reported differences between PEEK and PSU are now easily explainable. First, the dose for sol–gel transition is lower for PSU than for PEEK. Since

$$\delta_G = \frac{2.10^7}{M_{W0}.[4G(x) - G(s)]} \tag{36}$$

$$\frac{(\delta_G)_{PEEK}}{(\delta_G)_{PSU}} = \frac{(M_{W0})_{PSU}.[4G(x) - G(s)]_{PSU}}{(M_{W0})_{PEEK}.[4G(x) - G(s)]_{PEEK}} \tag{37}$$

Using $(M_{W0})_{PEEK} = 25\ kg\ mol^{-1}$, $G(x)_{PEEK} = 0.024$, $G(s)_{PEEK} \approx 0$ and $G(s)_{PSU} \approx G(x)_{PSU} \approx 0.15$, gives

$$(\delta_G)_{PEEK} \approx 8(\delta_G)_{PSU}$$

Gelation is thus expected to occur at lower dose for PSU than for PEEK in good agreement with our experimental observations. A possible explanation is that radiochemical yield for radical formation is higher for PSU than for PEEK, which will be discussed in the following.

Second, sol–gel transition is more progressive in PEEK than in PSU. It is also noteworthy that gelation is completed at high dose for PSU whereas a soluble fraction remains in PEEK even after 30.7 MGy irradiation. A possible explanation comes from the sample geometry: the TOL is about 25% of the whole thickness in PEEK whereas it is about 10% in PSU.

Third, the relatively large compilation of radiochemical yield values made by Horie and Schnabel[38] shows that aliphatic polysulfones are among the less stable polymers with $G(s)$ values of the order of 10. High yields of SO_2 are observed, thus indicating the probable occurrence of the weak[39,40] carbon–sulfone bond cleavage. It seems reasonable to suppose that such is the case also for PSU even though the yield is considerably lower owing to the well-known protective effect of aromatic nuclei evidenced for instance in studies on isobutylene–styrene[41] or acrylate–styrene[42] copolymers for which radiochemical stability increases with aromatic content, increased stability of phthalate-plasticized poly(vinyl chloride),[43] or polymer radioprotection by polyaniline.[44]

A higher radical yield for PSU than PEEK was also shown by the results of Heiland *et al*.[45] Those authors measured the radical concentration *versus* irradiation dose. It can be demonstrated that

$$G(P^\bullet) = 10^7 \times \left(\frac{d[P^\bullet]}{dt}\right)_{t\to 0} \tag{38}$$

Thus, one obtains $G(P^\bullet)_{PSU} \approx 0.75$ and $G(P^\bullet)_{PEEK} \approx 0.25$.

On the PSU radiochemical oxidation mechanism

Let us now try to establish a possible radiochemical degradation mechanism consistent with

- the sudden sol–gel transition;
- the H-crosslinking mechanism;
- the nature of carbonyl compounds and the possible appearance of SO_x–H detected by transmission FTIR.

First, the bond dissociation energies of PSU repeat constitutive units are shown in Fig. 13.[39–40] These values are consistent with the negative role of the SO_2 moiety.[46] They also suggest the possible role of isopropylidene groups in a radical chain mechanism.

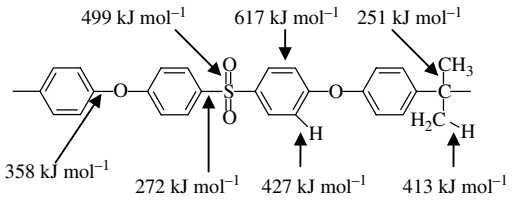

Figure 13. Constitutive repetitive unit of PSU and bond dissociation energies.

- Primary alkyl radicals are likely generated by PSU radiolysis:

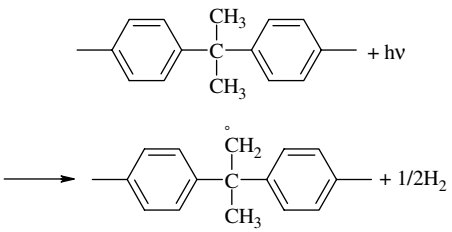

- Some tertiary radicals come from methane ejection the occurrence of this (minor) mechanism seems backed up by the measurement of a low methane emission yield by Brown and O'Donnell:[3]

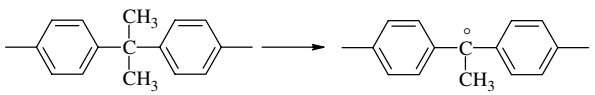

- Aryl radicals are no doubt also generated. However, their reactivity is probably lower than the reactivity of tertiary and especially primary alkyl radicals, which explains the lower PSU stability compared with PEEK, and also the suddenness of the sol–gel transition.

Sulfone groups are possibly involved in the following initiation mechanism:

$$P{-}SO_2{-}P + h\nu \longrightarrow [P{-}SO_2{-}P]^* \quad \text{(I)}$$

$$2[P{-}SO_2{-}P]^* \longrightarrow \text{inactive products} \quad \text{(II)}$$

$$[P{-}SO_2{-}P]^* \longrightarrow [P{-}SO_2^{\bullet} + P^{\bullet}]_{cage} \quad \text{(III)}$$

$$\text{Cage recombination}: [P{-}SO_2^{\bullet} + P^{\bullet}]_{cage} \longrightarrow [P{-}SO_2{-}P] \quad \text{(IV)}$$

$$[P{-}SO_2^{\bullet} + P^{\bullet}]_{cage} \longrightarrow P{-}SO_2^{\bullet} + P^{\bullet} \quad \text{(V)}$$

$$PSO_2^{\bullet} \longrightarrow P^{\bullet} + SO_2\nearrow \quad \text{(VI)}$$

The $G(s)$ value[2,3] is greater than the $G(SO_2)$ value. This indicates that a minor part of $PSO_2^{\bullet}$ generated in reaction (III) will generate SO_2 by reaction (VI). The other part reacts possibly by abstracting hydrogen to give a sulfonic acid eventually oxidized to give a sulfate. This statement is in good agreement with the shape of FTIR spectra displaying an absorption that could be ascribed to sulfonic acid derivatives.

According to Brown and O'Donnell,[3] $G(s)$ increases with temperature in the glassy state but becomes zero in the rubbery one. A possible explanation is that the segmental mobility increases with temperature in the glassy state which favours the escape of radicals from the cage (reaction (V)) compared with recombination. In the rubbery state, cooperative motions of large amplitude would favour the quenching of the excited state by bimolecular mechanisms (reaction (II)).

Brown and O'Donnell[3] also found that the radiochemical yield for crosslinking $G(x)$ is higher in the rubbery state (0.67 at 220 °C) than in the glassy state (0.25 at 125 °C). A similar trend was observed for polyethersulfone by Li *et al.*[6] Those authors reported a T_g increase for irradiation under nitrogen in the rubbery state and a T_g decrease for irradiation in the glassy state. These results would be difficult to reconcile with the preceding one if the excited state $[P{-}SO_2{-}P]^*$ was responsible for crosslinking.

It is reasonable to assume that H-crosslinking originates from the radiolysis of methylene groups:

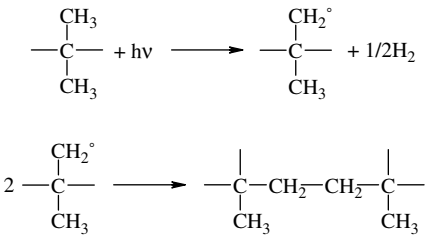

Indeed, such radical coupling would be favoured by a molecular mobility increase, especially by the 'valence migration process':[47]

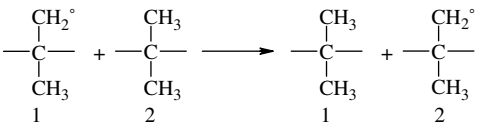

Hydrogen abstraction by $H^{\bullet}$ radicals can also propagate the reaction over relatively long distances.

If oxygen is present, it will inhibit efficiently all these processes provided the sample is oxygenated enough. The formation of various carbonyl species can then be explained from reaction between oxygen and the various alkyl radicals.

- The hydrogen abstraction of $-CH_2-H$ leading to an aldehyde absorbing at 1725 cm^{-1}:

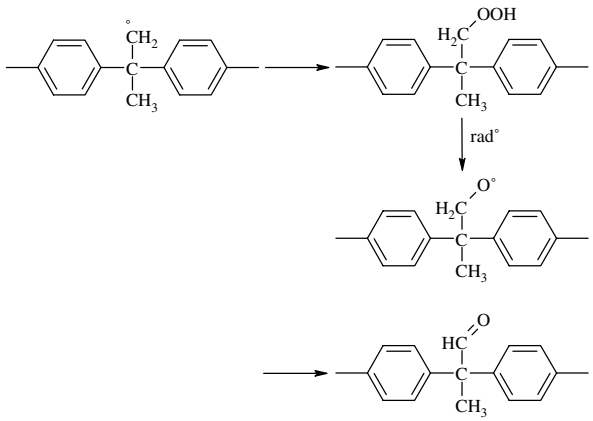

- The radiochemical cleavage of $\rightarrow C-CH_3$ bond leading to an acetophenone absorbing at 1690 cm^{-1}:

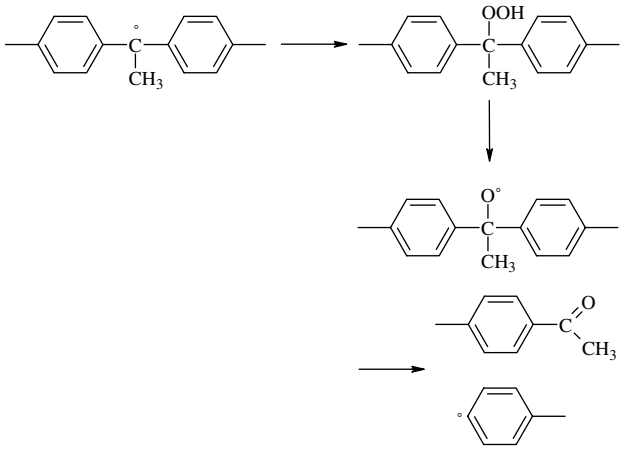

- Note that methyl ketones are also formed from a possible primary alkyl radical rearrangement leading to a tertiary one as reported by Rivaton for PC.[48]
- The existence of benzo-1,2-quinone generated by β-scission of aromatic alkoxy was suggested for PEEK[10] and seems also possible for PSU.

$G(x)$ and $G(s)$ values in the absence of oxygen are very close (0.15). This suggests a value of the same order of magnitude for the radical formation $G(P^{\bullet})$. For example, Brown and O'Donnell[2] measured $G(SO_2) = 0.018$, $G(H_2) = 0.007$, $G(x) = 0.05$, so that $G(P^{\bullet}) = 2(G(x) + G(H_2) + G(SO_2)) \approx 0.15$. Finally, $G(P^{\bullet})$ ranges from 0.15 (interpretation of Brown and O'Donnell's results) to 0.75 (interpretation of results of Heiland *et al*.) and G_{OX} is close to 1.5. Consequently, the kinetic chain length for hydroperoxidation ranges from 2 to 10, but in any case higher than unity which demonstrates unambiguously the occurrence of significant branching.

CONCLUSIONS

Basically put, PSU belongs to a family of polymers that are quite stable (compared with aliphatic polymers) to ionizing radiations, owing to its relatively high aromatic character. However, its stability is significantly lowered by the presence of both sulfone and isopropylidene groups.

- Sulfone groups are presumably responsible for the primary chain scissions that occur even in the absence of oxygen. The corresponding yield value would be of the order of 0.15.
- Isopropylidene groups are probably responsible for the crosslinking and perhaps some additional chain scissions in the absence of oxygen. Both crosslinking and chain scissions would be inhibited by oxygen but one cannot exclude the occurrence of secondary chain scissions resulting from hydroperoxide decomposition.

The results presented above confirm previously described diffusion-limited oxidation for radiochemical ageing: fully oxygenated (thin) samples undergo mainly chain scissions whereas anaerobic degradation of thick samples generates crosslinking. This work illustrates this behaviour by the study of structural changes at the macromolecular scale using:

- rheometric properties and gel content formation for detecting crosslinking;
- GPC and T_g measurements for detecting and quantifying chain scissions, noting that the values employed for universal calibration and the Fox–Flory law have not been reported before to our knowledge; and
- micro-ATR, which is confirmed to be an efficient analytical tool for TOL measurements with a precision of the order of 2 μm and with the advantage of simplicity of measurement.

The TOL is about 100 μm in air for a dose rate close to 6.67 Gy s^{-1}. According to classical kinetic models, the rate for oxygen consumption r_{OX} can be approximated by a power law:

$$r_{OX} \propto I^n \tag{39}$$

where I is the dose rate and n ranges between 0.5 (long kinetic chain)[49,50] and 1 (short kinetic chain).[51] This means that the TOL can also be approximated by a power law:

$$TOL \propto I^{-n/2} \tag{40}$$

For a dose rate 100 times lower, the TOL would be 3 to 10 times greater. The consequences of such a dependence on mechanical properties need to be investigated.

The work reported indicates the predominance of H-crosslinking for the conditions under study but knowledge of conditions favouring whether H- or Y-crosslinking occurs remains an open question.

ACKNOWLEDGEMENTS

The authors are grateful to EDF for financial support, Solvay for supplying the PSU, Hans Ooms and Serge Brichard from SCK-CEN laboratory (Mol, Belgium) for performing irradiations and Paulo Ferreira (PIMM) for PSU processing.

REFERENCES

1 Hill DJT, Kudoh H and Seguchi T, *Radiat Phys Chem* **48**:569–576 (1996).
2 Brown JR and O'Donnell JH, *J Appl Polym Sci* **19**:405–417 (1975).
3 Brown JR and O'Donnell JH, *J Appl Polym Sci* **23**:2763–2775 (1979).
4 Hill DJT, Lewis DA and O'Donnell JH, *J Appl Polym Sci* **44**:115–120 (1992).
5 Hill DJT, Lewis DA, O'Donnell JH and Whittaker AK, *Polym Adv Technol* **9**:45–51 (1998).
6 Li J, Oshima A, Miura T and Washio M, *Polym Degrad Stab* **91**:2867–2873 (2006).
7 Stephan M, Pospiech D, Heidel R, Hoffmann T, Voigt D and Dorschner H, *Polym Degrad Stab* **90**:379–385 (2005).
8 Claudy P, Letoffé JM, Camberlain Y and Pascault J, *Polym Bull* **9**:208–215 (1983).
9 Commereuc S, Bonhomme S, Verney V and Lacoste J, *Polymer* **41**:917–923 (2000).
10 Richaud E, Ferreira P, Audouin L, Colin X, Verdu J and Monchy-Leroy C, *Eur Polym J* **46**:731–743 (2010).
11 Gutiérrez G, Fayolle B, Régnier G and Medina J, *Polym Degrad Stab* **95**:1708–1715 (2010).
12 Rivaton A and Gardette JL, *Polym Degrad Stab* **66**:385–403 (1999).
13 Grubisic Z, Rempp P and Benoit H, *J Polym Sci B: Polym Lett* **5**:753–759 (1967).
14 Yau WW, Kirkland JJ and Bly DD, Laboratory techniques, in *Modern Size-Exclusion Liquid Chromatography: Practice of Gel Permeation and Gel Filtration Chromatography*. John Wiley, New York, pp. 249–283 (1979).
15 Mills NJ, *Rheol Acta* **13**:185–190 (1974).
16 Ma Z, Kotaki M and Ramakrishna S, *J Membr Sci* **272**:179–187 (2006).

17 Charlesby A, *Atomic Radiation and Polymer*. Pergamon Press, Oxford, p. 68 (1960).
18 Saito O, *J Phys Soc Japn* **13**:198–206 (1958).
19 Rosiak JM, *Radiat Phys Chem* **51**:13–17 (1998).
20 Moad CL and Winzor DJ, *Prog Polym Sci* **23**:759–813 (1998).
21 Planes E, Chazeau L, Vigier G and Fournier J, *Polymer* **50**:4028–4038 (2009).
22 Jones RA, Groves DJ, Ward IM, Taylor DJR and Stepto RFT, *Nucl Instrum Meth Phys Res B* **151**:213–217 (1999).
23 Fox TG and Flory PJ, *J Appl Phys* **21**:581–591 (1950).
24 Simha R and Boyer RF, *J Chem Phys* **37**:1003–1007 (1962).
25 Bicerano J, Transition and relaxation temperatures, in *Prediction of Polymer Properties*, 3rd edition. Marcel Dekker, New York, pp. 169–259 (2002).
26 Linares A and Acosta JL, *J Appl Polym Sci* **92**:3030–3039 (2004).
27 Weber M and Heckmann W, *Polym Bull* **40**:227–234 (1998).
28 Shumsky VF, Lipatov YS, Kulichikhin VG and Getmanchuk IP, *Rheol Acta* **32**:352–360 (1993).
29 Jansen JA, *J Fail Anal Prev* **1**:55–58 (2001).
30 Shenoy AV, Saini DR and Nadkarni VM, *Rheol Acta* **22**:209–222 (1983).
31 Di Marzio EA, *J Res Nat B Stand A* **68A**:611–617 (1964).
32 Fox TG and Loshaek S, *J Polym Sci* **15**:371–390 (1955).
33 Winter HH and Chambon F, *J Rheol* **30**:367–382 (1986).
34 Audouin L, Langlois V, Verdu, J and Bruijn JCM, *J Mater Sci* **29**:569–583 (1994).
35 Van Krevelen DW, Permeation of polymers: the diffusive transport of gases, vapours and liquid in polymers, in *Properties of Polymers*, 3rd edition. Elsevier, New York, pp. 403–425 (1976).
36 Dély N, Ngono-Ravache Y, Ramillon JM and Balanzat E, *Nucl Instrum Meth Phys Res B* **236**:145–152 (2005).
37 Denisov ET and Afanas'ev IB, Chain mechanism of liquid phase oxidation of hydrocarbons, in *Oxidation and Antioxidants in Organic Chemistry and Biology*. Taylor and Francis/CRC Press, Boca Raton, FL, pp. 23–83 (2005).
38 Horie K and Schnabel W, *Polym Degrad Stab* **8**:145–159 (1984).
39 Li XG and Huang MR, *React Funct Polym* **42**:59–64 (1999).
40 Molnár G, Botvay A, Pöppl L, Torkos K, Borossay J, Máthé Á, *et al*., *Polym Degrad Stab* **89**:410–417 (2005).
41 Alexander P and Charlesby A, *Nature* **173**:587–579 (1954).
42 Kellman R, Hill DJT, O'Donnell JH and Pomery PJ, *Am Chem Soc Polym Prepr* **31**:391–392 (1990).
43 Thominette F, Metzger G, Dalle B and Verdu J, *Eur Polym J* **27**:55–59 (1991).
44 Ismail MN, Ibrahim MS and Abd El-Ghaffar MA, *Polym Degrad Stab* **62**:337–341 (1998).
45 Heiland K, Hill DJT, Hopewell JL, Lewis DA, O'Donnell JH, Pomery PJ, *et al*., *Adv Chem Ser* **249**:637–649 (1996).
46 Lewis A, O'Donnell JH, Hedrick JL, Ward TC and McGrath JEE, Radiation-resistant, amorphous, all-aromatic poly(arylene ether sulfones): synthesis, physical behavior, and degradation characteristics, in *The Effects of Radiation on High-Technology Polymers*, ed. by Reichmanis E and O'Donnell JH. American Chemical Society, Washington, DC, pp. 252–261 (1989).
47 Emanuel NM and Buchachenko AL, Migration of reactive species, in *Chemical Physics of Polymer Degradation and Stabilization*, *New Concepts in Polymer Science*, ed. by de Jonge CHRI. VNU Science Press, Utrecht, pp. 81–118 (1990).
48 Rivaton A, *Polym Degrad Stab* **49**:163–179 (1995).
49 Wise J, Gillen KT and Clough RL, *Polymer* **38**:1929–1944 (1997).
50 Wise J, Gillen KT and Clough RL, *Radiat Phys Chem* **49**:565–573 (1997).
51 Decker C, Mayo FR and Richardson H, *J Polym Sci: Chem Ed* **11**:2879–2898 (1973).